Princeton Plasma Physics Laboratory

PPPL-5210

Full-wave modeling of EMIC waves near the He^+ gyrofrequency

Eun-Hwa Kim and Jay R. Johnson

November 2015

Prepared for the U.S. Department of Energy under Contract DE-AC02-09CH11466.

Full-wave modeling of EMIC waves near the He^+ gyrofrequency

Eun-Hwa Kim[1] and Jay R. Johnson[1]

Corresponding author: E.-H. Kim, Princeton Center for Heliophysics and Princeton Plasma Physics Laboratory, Princeton University, P.O. Box 0451, Princeton, NJ 08543-0451, USA (ehkim@pppl.gov)

[1] Princeton Center for Heliophysics and Princeton Plasma Physics Laboratory, Princeton University, Princeton, New Jersey, USA

Abstract

Electromagnetic (EMIC) waves are known to be excited by the cyclotron instability associated with hot and anisotropic ion distributions in the equatorial region of the magnetosphere and are thought to play a key role in radiation belt losses. Although detection of these waves at the ground can provide a global view of the EMIC wave environment, it is not clear what signatures, if any, would be expected. One of the significant scientific issues concerning EMIC waves is to understand how these waves are detected at the ground. In order to solve this puzzle, it is necessary to understand the propagation characteristics of the field-aligned EMIC waves, which include polarization reversal, cutoff, resonance, and mode coupling between different wave modes, in dipolar magnetic field. However, the inability of ray-tracing to adequately describe wave propagation near the crossover cutoff-resonance frequencies in multi-ion plasma is a one of reasons why the scientific questions remain unsolved. Using a recently developed 2D full-wave code that solves the full wave equations in global magnetospheric geometry, we demonstrate how EMIC waves propagate from the equatorial region to higher magnetic latitude in an electron-proton-He^+ plasma. We find that polarization reversal occurs at the crossover frequency from left-hand (LHP) to right-hand (RHP) polarization and such RHP EMIC waves can either propagate to the inner magnetosphere or reflect to the outer magnetosphere at the Buchsbaum resonance location. We also find that mode-coupling from guided LHP EMIC waves to unguided RHP or LHP waves (i.e., fast mode) occurs.

1. Introduction

For decades, ultra-low frequency (ULF) electromagnetic ion cyclotron (EMIC) waves in the Pc 1-2 frequency range have been observed as a prominent feature in the magnetosphere and ionosphere, and these waves play an important role on radiation belt and ring current particles [e.g., *Loto'aniu et al.*, 2006; *Shprits et al.*, 2006; *Jordanova et al.*, 2008; *Miyoshi et al.*, 2008; *Albert* and *Bortnik*, 2009; *Thorne*, 2010].

Conjugate ground-satellite observations have suggested that EMIC waves originating in the equatorial magnetosphere could propagate from the equator to the ionosphere [e.g., *Perraut et al.*, 1984; *Anderson et al.*, 1992a, 1992b, 1996; *Erlandson et al.*, 1990; *Erlandson* and *Anderson*, 1996; *Hansen et al.*, 1995]. These observations have provided significant challenge to modeling efforts. Many theoretical analyses made use of the ray-tracing technique, which has provided the first step in understanding the nonlocal features of EMIC waves. Using this method, *Rauch* and *Roux* [1982] found that the waves should reflect at the Buchsbaum resonance (or bi-ion frequency) [*Buchsbaum*, 1960] and would not reach ionospheric altitudes. This work was extended to warm plasmas with similar results [e.g., *Horne* and *Thorne*, 1990; *Rönnmark* and *André*, 1991; *Chen et al.*, 2014]. However, these results are inconsistent with the conjugate studies noted above.

On the other hand, a 1D full-wave analysis [*Johnson et al.*, 1989; *Johnson* and *Cheng*, 1999] found that equatorially generated EMIC waves could reach the ground via polarization reversal at the crossover location, wave tunneling through the evanescent region, and mode conversion process near the additional heavier ion gyrofrequency, respectively. Simulations using a 2D hybrid code [*Hu et al.*, 2010] also presented good agreement with *Johnson and Cheng* [1999] showing wave tunneling for small heavy ion density concentration.

However, these modeling efforts could only describe partial characteristics of EMIC wave propagation because ray tracing cannot describe wave mode conversion/coupling and tunneling effect and the 1D full-wave calculations did not include 2D magnetic curvature effects. A recently developed 2D full-wave (hereafter FW2D) code using finite element method [*Kim et al.*, 2015a] overcomes these shortcomings using an approach that describes wave propagation, mode conversion and tunneling with 2D magnetic curvature effect for arbitrary plasma and magnetic field configurations.

In this letter, we use the FW2D code to examine EMIC wave propagation at Earth by adopting dipole magnetic field configuration and empirical density model [*Sheeley et al.*, 2001; *Denton et al.*, 2006]. In particular, we examine the effects of wave normal angle on EMIC wave propagation in order to address the recent observational findings that EMIC waves typically have a range of normal angle up to 60°, even at the magnetic equator where most EMIC waves are believed to be generated [*Min et al.*, 2012; *Allen et al.*, 2015; *Saikin et al.*, 2015]. The results in this letter show that propagation of EMIC waves depends sensitively on wave normal angle, and for certain conditions, the waves can propagate to the inner (thus possibly reach the ionospheric altitude) or outer magnetosphere.

The paper is structured as follows: a brief wave dispersion characteristic along the magnetic field is illustrated in Section 2. Section 3 contains 2D full-wave simulation results showing wave propagation along the field line and polarization reversal and mode conversion at the crossover location. The last section contains a brief discussion and summary.

2. Wave coupling near the heavy ion gyrofrequencies

Wave properties in multi-ion plasmas are well known [e.g., *Smith* and *Brice*, 1964; *Young et al.*, 1981; *Rauch* and *Roux*, 1982; *Johnson et al.*, 1989, 1995]. Following *Johnson et al.* [1995], we illustrate wave dispersion relation along the field line at L=7.2 as shown in Figure 1. For this calculation, we adopt an electron-H^+-He^+ plasma with constant ion density concentration ratios of $\chi_{He} = N_{He}/N_e$ = 5%, where N_j is a number density of jth particle. We adopt an empirical electron density model in power law dependence [e.g., *Denton et al.*, 2006],

$$N_e = N_{e0}\left(\frac{LR_E}{R}\right)^{\alpha}, \tag{1}$$

where R is radial distance and LR_E is a geocentric radius at the magnetic equator based on dipole magnetic field model, $\alpha = 0.8$ is a constant depending on location [*Denton et al.*, 2006], and N_{e0} is the value of N_e at the magnetic equator [*Sheeley et al.*, 2001],

$$N_{e0} = 1390\left(\frac{3}{L}\right)^{4.83}. \tag{2}$$

For simplicity, Earth's magnetic field is assumed to be a dipole, where the equatorial magnetic field strength at Earth's surface is B_s =3.0 ×10^{-5} T,

$$B_0 \cong \frac{B_S}{R^3}\sqrt{1+3\sin^2\Lambda}, \tag{3}$$

where Λ is a geomagnetic latitude.

We then calculate the critical frequencies between the H^+ (Ω_H) and He^+ (Ω_{He}) gyro-frequencies such as the crossover frequency ($\omega^2_{cr} = \chi_{He}\Omega^2_H + \chi_H\Omega^2_{He}$), the Buchsbaum resonance frequency ($\omega^2_{bb} = \Omega_H\,\Omega_{He}\,(\chi_{He}\Omega_H + \chi_H\Omega_{He})/\,(\chi_{He}\Omega_{He} + \chi_H\Omega_H)$), and the LHP wave cutoff frequency ($\omega_{Lcut} = \chi_{He}\Omega_H + \chi_H\Omega_{He}$), respectively. Because these frequencies are function of $|\mathbf{B}_0|$ and heavy ion density ratio (χ_{ion}), the frequencies increase as Λ increases for constant χ_{He}, as shown in Figure 1a.

Figure 1b shows the wave dispersion relation as a function of magnetic latitude (Λ) and wavelength ($\lambda = 2\pi / k$, where k is a wavenumber) for wave frequency $\omega = 2\pi f = 3.2$ Hz and θ_k =25°, where θ_k is a wave normal angle between **k** and $\mathbf{B}_0$. When waves propagate oblique to $\mathbf{B}_0$, the dispersion relation for two-ion plasma is characterized by three separate modes, which are labeled Class I, II, and III.

Class I, which is the magnetosonic branch, has frequencies $\omega > \omega_{\mathrm{Lcut}}$ at lower magnetic latitude $\lambda < 22.7°$. Polarization reversal occurs where $\omega = \omega_{\mathrm{cr}}$, such that waves with $\omega > \omega_{\mathrm{cr}}$ are RHP, while they are LHP for $\omega_{\mathrm{Lcut}} < \omega < \omega_{\mathrm{cr}}$. Class II is the H^+ cyclotron branch, which can be excited near the magnetic equator and propagate along the magnetic field toward higher latitude and increasing magnetic field strength. At the point where $\omega = \omega_{\mathrm{cr}}$, these waves should reverse polarization from LHP to RHP. Once the waves become RHP, they continue to be guided to the location where $\omega = \omega_{\mathrm{bb}}$ and the waves become unguided for $\omega < \omega_{\mathrm{bb}}$ [*Rauch and Raux*, 1982]. The 1D full wave calculation by *Johnson and Cheng* [1999] showed that the RHP wave could mode-convert to the Class III mode, which is a guided LHP cyclotron wave branch below Ω_{He}, and finally reach the ground. At the crossover location, mode conversion between Class I and II can also occur [e.g., *Smith* and *Brice*, 1964; *Johnson et al.*, 1995]. *Johnson et al.* [1995] demonstrated that there is mode conversion θ_k window where the modes can be coupled.

3. Wave Solutions at Earth's magnetosphere

In order to examine plasma waves in arbitrary magnetosphere, *Kim et al.* [2015a] recently developed the FW2D code, which is a 2D full-wave code using finite element method. This code describes the three-dimensional wave structure when plasma waves are launched in a two-dimensional axisymmetric background plasma with arbitrary magnetic field topology. In this code, the perturbed electric field is expressed in coordinates aligned along and across the local magnetic field ($\mathbf{B}_0$) direction ($\boldsymbol{\eta}$, $\boldsymbol{\varphi}$, and $\mathbf{b}$), where $\mathbf{b} = \mathbf{B}_0/|\mathbf{B}_0|$ is the unit vector along the magnetic field line, $\boldsymbol{\varphi}$ is the azimuthal direction, and $\boldsymbol{\eta}$ is normal to the field line pointing outward ($\boldsymbol{\eta} = \boldsymbol{\varphi} \times \mathbf{b}$).

For calculations, we adopt an empirical electron density model as shown in equations (1)-(2) and Earth's magnetic field is assumed to be a dipole as shown in equation (3). Because He^+ is one of the primary ions in Earth's magnetosphere and waves are often observed between the He^+ (Ω_{He}) and H^+ (Ω_H) gyro-frequencies [e.g., *Saikin et al.*, 2015], we adopt an electron-H^+-He^+ plasma and for simplicity specify χ_{He}=5%. Waves with ω=3.2 Hz (between the local Ω_{He} and Ω_H frequencies) are launched near the magnetic equator along the field line at L=7.2. For this study, we limit the computational domain ($4.75<r/R_E<7.75$ and $-3.5<z/R_E<3.5$) using absorbing boundary conditions (which only allows outgoing wave solutions) at the edge of the solution domain as shown in Figure 2a.

The density of the mesh can be specified based on the expected wavelength obtained from the solution of the local dispersion except when close to resonances (thus $\lambda \rightarrow 0$), so that the most efficient resolution is used. Figure 2a gives a schematic illustration of a nonuniform and unstructured triangular mesh. Because we focus on wave propagation along $\mathbf{B}_0$ near L=7.2, a fine mesh is adopted in that area. Depending on the spatial scale of the dispersive effect, we use a more refined mesh than that illustrated Figure 2a to resolve all relevant structures. For example, the total nodes for the wave solutions presented in this paper is 91384 compared with the 1747 nodes shown in Figure 2a.

In order to examine how the wave normal angle near the magnetic equator affects to EMIC wave propagation, we perform two simulations with wide (Case A) and narrow (Case B) source width in the **η** direction as shown in Figure 2b and 2c, respectively. Because the width of the source is closely related to the initial wavevector in the **η** direction, which is perpendicular to the magnetic field, these two cases correspond to different initial wave normal angles with the narrow source corresponding to more oblique and the wide source as more field-aligned. For both cases, we give the initial field-aligned wavelength of $\lambda_b \sim 0.1$ R_E, which is similar to the wavelength calculated from the dispersion relation of LHP Class II waves at $\Lambda = 0^{\circ}$ as shown in Figure 1c. The circularly polarized electric field components perpendicular to $\mathbf{B}_0$ can be calculated using E_η and E_φ,

$$E_{RH(LH)} = \left(E_\eta \pm iE_\phi\right)/\sqrt{2}\,, \tag{4}$$

and we launch LHP waves using this equation. In our calculations, the azimuthal wave number of the source is assumed to be 0 for simplicity.

In Figure 2b and 2c, we also plot the critical locations, such as l_{He}, l_{bb}, l_{Lcut}, and l_{cr}, where wave frequency matches the critical frequencies of Ω_{He}, ω_{bb}, ω_{Lcut}, and ω_{cr}, respectively. Because the crossover is located at the lowest magnetic latitude, when waves propagate from the magnetic equator to the higher Λ, waves first encounter l_{cr} then pass through l_{Lcut}, l_{bb}, and l_{He}, respectively.

Figure 3 and Figure 4 show the wave solutions in the magnetosphere of the fluctuating electric (**E**) fields, the Poynting flux, and ellipticity for Case A and B, respectively. When waves propagate quasi-parallel to $\mathbf{B}_0$ for Case A in Figure 3, wavefronts are nearly perpendicular to the magnetic field lines thus, the wave normal angle is almost 0°. These waves are well guided along $\mathbf{B}_0$ and propagate toward regions where $|\mathbf{B}_0|$ increases as indicated by the direction of the Poynting flux shown in Figure 3e and 3f. As these waves propagate along $\mathbf{B}_0$ and slightly toward higher L-shell, wave refraction occurs due to the magnetic curvature and thus wave polarization rapidly changes from LHP to linear. However, the inner edge of the ray shows polarization reversal at the crossover location in Figure 3g. When waves reach the Buchsbaum resonance location (l_{bb}), the wave normal angle, θ_k, becomes nearly 90°, and waves reflect toward higher L-shell and lower magnetic latitude, which is consistent with ray tracing calculations [e.g., *Chen et al.*, 2014] and hybrid simulations [*Denton et al.*, 2014], with linear polarization. For the given condition, there is no wave tunneling from H^+-band to He^+-band EMIC waves.

When waves propagate with larger wave normal angle as in Case B shown in Figure 4, we found that there are two strong rays propagating toward smaller (red arrow in Figure 4a and 4f) and larger L-shell (blue arrow in Figure 4a and 4f), respectively. For both rays, the wavefronts are tilted relative to the local magnetic field line direction. The wave normal angle can be estimated from the wave solutions as the angle between the normal to the wavefronts and the magnetic field line and for the given solution, the wave normal angles near the magnetic equator are roughly ~40° for waves propagating toward lower L-shell and ~50° for waves propagating toward larger L-shell, respectively. Both rays are also strongly guided by $\mathbf{B}_0$ and propagate toward higher magnetic latitude, however, the two rays have different propagation characteristics.

The characteristics of the outer ray at larger L-shell are similar to Figure 3. Field-aligned waves propagate to higher magnetic latitude, reach the Buchsbaum resonance, and reflect. The polarization changes rapidly from LHP to linear. However, for waves propagating toward smaller L-shell, there is evidence of wave mode conversion and polarization reversal at l_{cr}. When waves encounter l_{cr}, mode conversion from earthward propagating LHP EMIC waves to magnetosonic waves occurs as shown in Figure 4b. The RHP magnetosonic waves (marked A in Figure 4b) propagate to the weaker magnetic field region (outer magnetosphere), while LHP magnetosonic waves propagate to the stronger magnetic field region from l_{cr} to l_{Lcut} where they reflect and propagate to the outer magnetosphere (marked “B” in Figure 4b). At l_{cr}, polarization reversal from LHP to RHP also occurs. When RHP EMIC wave modes reach l_{bb}, these waves become unguided as shown in Figure 4 and disperse into the inner/outer magnetosphere (marked “C” and “D” in Figure 4b).

For wave propagation to smaller L-shell, Figure 4 does not show a strong polarization reversal at l_{cr} because of the existence of strong mode coupling from LHP Class II to the LHP magnetosonic mode. The strong, unguided wave mode in the inner magnetosphere provides clear evidence of polarization reversal. For a ray propagating toward higher L-shell, we found that ellipticity shows strong RHP between l_{cr} and l_{Lcut} where quasi-linear polarization of the field-aligned mode and reflecting RHP magnetosonic waves at l_{Lcut} are mixed.

Based on the eigenmode solution shown in Figure 3 and Figure 4, we reproduce time-dependent wave solutions, such as,

$$E(r,z,t) = E(r,z)\exp(-i\omega t), \tag{5}$$

as shown in Movie S1-S2. The Movie S1 and S2 clearly show how LHP EMIC waves propagate from the magnetic equator to the higher magnetic latitudes in time.

4. Discussion and Summary

In this letter, we present how LHP EMIC waves, which are generated near the magnetic equator, propagate along the magnetic field line. We show excellent agreement with previous calculations, such as EMIC wave cutoff at the Buchsbaum resonance [e.g., *Rauch* and *Roux*, 1982], polarization reversal [e.g., *Johnson and Cheng*, 1999] and mode conversion [*Johnson et al.*, 1995] at the crossover locations.

The simulation results show that equatorially generated EMIC waves can propagate into the inner or outer magnetosphere depending on the wave normal angle, and thus we suggest that wave normal angle could be one of the important parameters that control EMIC wave propagation to the ground. Recent statistical studies [e.g., *Min et al.*, 2012; *Allen et al.*, 2015; *Saikin et al.*, 2015] indicated that EMIC waves have a variety of wave normal angles. In the outer magnetosphere ($L > 8$), wave normal angles in the dawn sector are significantly larger than in the dusk and noon sectors. According to hybrid simulations [*Hu et al.*, 2010], LHP EMIC waves can be generated with a large wave normal angle when plasma contains little He^+ density. However, how the wave normal angle is related to characteristics of EMIC wave propagation remains largely unexplored.

We also found that mode-conversion from the LHP EMIC to magnetosonic waves clearly occurs at the crossover location when the wave vector becomes nearly parallel to the local magnetic field line, consistent with *Johnson et al.* [1995]. When waves propagate toward smaller L-shell in Figure 4, they reach the crossover location near L~7.15 and wavefronts are approximately normal to the local magnetic field line. For waves propagating to larger L-shell in Figure 3 and Figure 4, the wave normal angle increases as Λ increases and no mode conversion at the crossover location occurs. For instance, waves in Figure 3 have normal angle approximately 63° at the crossover location. Because of the limitations of ray tracing [e.g., *Chen et al.*, 2014], 1D full-wave model [*Johnson and Cheng*, 1999], or 1D time-dependent wave model [*Kim and Lee*, 2005], such mode conversion has not been found in previous numerical simulations of field-aligned propagation waves. This strong mode conversion provides an additional EMIC wave energy loss mechanism and suggests the need for further investigation.

Very recently, the DEMETER satellite detected EMIC waves that are believed to be generated at plasmapause or plasmasphere and propagate to the topside ionosphere as RHP waves in wide range of L-shell [*Píša et al.*, 2015]. Our results in Figure 4 strongly support such observations.

RHP Class II EMIC waves propagating toward lower L-shell in Figure 4 become unguided for $\omega<\omega_{bb}$, thus these waves could be simultaneously detected at different L-shell in the inner magnetosphere. Such waves can also be generated between the O^+ and He^+ gyro-frequencies, and can propagate to the inner magnetosphere as unguided RHP waves when wave frequency becomes lower than the Buchsbaum resonance frequency.

Although the presence of O^+ ion impacts the generation and propagation of the waves in the ion cyclotron frequency range [e.g., *Silin et al.*, 2011; *Gary et al.*, 2012; *Chen et al.*, 2013; *Omidi et al.*, 2013; *Denton et al.*, 2014; *Lee* and *Angelopoulos*, 2015; *Min et al.*, 2015], we assume a constant heavy ion density concentration ratio throughout the calculation domain which is similar to previous numerical studies [e.g., *Johnson* and *Cheng*, 1999; *Chen et al.*, 2009; *Omidi et al.*, 2013].

When the heavy ion density concentration ratio varies along the magnetic field line, the mode conversion efficiency from incoming EMIC waves to magnetosonic waves and wave tunneling near the heavier ion cyclotron resonance are affected by the local heavy ion concentration ratio. For instance, when the heavier ion density increases, the cutoff condition for the field-aligned waves, such as the Buchsbaum resonance, shifts toward the outer magnetosphere and lower magnetic latitude. Thus the wave stopgap between the Buchsbaum resonance and heavier ion gyrofrequency locations becomes wider.

As shown by *Johnson and Cheng* [1999], O^+ can play an important role in EMIC wave propagation from the magnetic equator to the ground. The simulation in Figure 4 particularly shows that additional heavier ions are necessary for EMIC wave propagation to the ground. For the conditions explored in this paper, we find that EMIC waves at higher L-shell cannot tunnel through the evanescent region, only unguided RHP waves propagate to the inner magnetosphere.

Therefore, additional mode conversion from RHP waves to field-aligned waves, such as mode conversion at the ion-ion hybrid resonance [e.g., *Lee et al.*, 2008, *Kim et al.*, 2008, 2015a, 2015b, 2015c] may be necessary.

Acknowledgements. Authors thank Prof. Dong-Hun Lee and Dr. Hyomin Kim for useful discussion. The work at the Princeton University was supported by NASA grants (NNH09AM53I, NNH09AK63I, NNH11AR07I, NNX14AM27G, and NNH14AY20I), NSF grant ATM0902730, AGS-1203299 and DOE contract DE-AC02-09CH11466. This work was facilitated by the Max Planck/ Princeton Center for Plasma Physics.

References

Albert, J. M. and J. Bortnik (2009), Nonlinear interaction of radiation belt electrons with electromagnetic ion cyclotron waves, *Geophys. Res. Lett.*, *36*, L12110, doi:10.1029/2009GL038904.

Allen, R. C., J.-C. Zhang, L. M. Kistler, H. E. Spence, R.-L. Lin, B. Klecker, M. W. and André, M. Dunlop and V. K. Jordanova (2015), A statistical study of EMIC waves observed by Cluster: 1. Wave properties, *J. Geophys. Res. Space Phys.*, *120*, doi:10.1002/2015JA021333.

Anderson, B. J., R. E. Erlandson and L. J. Zanetti (1992a), A statistical study of Pc 1-2 magnetic pulsations in the equatorial magnetosphere 1. Equatorial occurrence distributions, *J. Geophys. Res.*, *97*, 3075-3088.

Anderson, B. J., R. E. Erlandson and L. J. Zanetti (1992b), A statistical study of Pc 1-2 magnetic pulsations in the equatorial magnetosphere 2. Wave properties, *J. Geophys. Res.*, *97*, 3089-3101.

Anderson, B. J., R. E. Erlandson, M. J. Engebretson, J. Alford and R. L. Arnoldy (1996), Source region of 0.2 to 1.0 Hz geomagnetic pulsation bursts, *Geophys. Res. Lett.*, *23*, 769-772.

Buchsbaum, S. J. (1960), Ion Resonance in a Multicomponent Plasma, *Phys. Rev. Lett*, *5*, 495-497.

Chen, L., R. M. Thorne and R. B. Horne (2009), Simulation of EMIC wave excitation in a model magnetosphere including structured high-density plumes, *J. Geophys. Res.*, *114*, A07221, doi:10.1029/2009JA014204.

Chen, L., R. M. Thorne, Y. Shprits and B. Ni (2013), An improved dispersion relation for parallel propagating electromagnetic waves in warm plasmas: Application to electron scattering, *J. Geophys. Res. Space Phys.*, *118*, 2185–2195, doi:10.1002/jgra.50260.

Chen, L., V. K. Jordanova, M. Spasojevic, R. M. Thorne and R. B. Horne (2014), Electromagnetic ion cyclotron wave modeling during the geospace environment modeling challenge event, *J. Geophys. Res.*, *119*, 2963–2977, doi:10.1002/2013JA019595.

Denton, R. E., K. Takahashi, I. A. Galkin, P. A. Nsumei, X. Huang, B. W. Reinisch, R. R. Anderson, M. K. Sleeper and W. J. Hughes (2006), Distribution of density along magnetospheric field lines, *J. Geophys. Res.*, *111*, 04213.

Denton, R. E., V. K. Jordanova and B. J. Fraser (2014), Effect of spatial density variation and O+ concentration on the growth and evolution of electromagnetic ion cyclotron waves, *J. Geophys. Res.*, *119*, 8372–8395, doi:10.1002/2014JA020384.

Erlandson, R. E. and B. J. Anderson (1996), Pc 1 waves in the ionosphere: A statistical study, *J. Geophys. Res.*, *101*, 7843–7857.

Erlandson, R. E., L. J. Zanetti, T. A. Potemra, L. P. Block and G. Holmgren (1990), Viking magnetic and electric field observations of Pc 1 waves at high altitudes, *J. Geophys. Res.*, *95*, 5941.

Gary, S. P., K. Liu and L. Chen (2012), Alfvén-cyclotron instability with singly ionized helium: Linear theory, *J. Geophys. Res.*, *117*, A08201, doi:10.1029/2012JA017740.

Hansen, H. J., B. J. Fraser, F. W. Menk and R. E. Erlandson (1995), Ground satellite observations of Pc 1 magnetic pulsations in the plasma trough, *J. Geophys. Res.*, *100*, 7971–7984.

Horne, R. B. and R. M. Thorne (1990), Ion cyclotron absorption at the second harmonic of the oxygen gyrofrequency, *Geophys. Res. Lett.*, *17*, 2225.

Hu, Y., R. E. Denton and J. R. Johnson (2010), Two-dimensional hybrid code simulation of electromagnetic ion cyclotron waves of multi-ion plasmas in a dipole magnetic field, *J. Geophys. Res.*, *115*, 9218, doi:10.1029/2009JA015158.

Johnson, J. R. and C. Z. Cheng (1999), Can ion cyclotron waves propagate to the ground?, *Geophys. Res. Lett.*, *26*, 671-674.

Johnson, J. R., T. Chang, G. B. Crew and M. Andre (1989), Equatorially generated ULF waves as a source for the turbulence associated with ion conics, *Geophys. Res. Lett.*, *16*, 1469-1472, doi:10.1029/GL016i012p01469.

Johnson, J. R., T. Chang and G. B. Crew (1995), A study of mode conversion in an oxygen-hydrogen plasma, *Phys. Plasmas*, *2*, 1274-1284.

Jordanova, V. K., J. Albert and Y. Miyoshi (2008), Relativistic electron precipitation by EMIC waves from self-consistent global simulations, *J. Geophys. Res.*, *113*, A00A10, doi:10.1029/2008JA013239.

Kim, E.-H. and D.-H. Lee (2005), Simulation Study of Electron and Proton whistlers in the Ionosphere, *J. Kor. Phys. Soc.*, *46*, 541-545.

Kim, E. -H., J. R. Johnson and D. -H. Lee (2008), Resonant absorption of ULF waves at Mercury's magnetosphere, *J. Geophys. Res.*, *113*, A11207.

Kim, E.-H., J. R. Johnson, E. Valeo and C. K. Phillips (2015a), Global modeling of ULF waves at Mercury, *Geophys. Res. Lett.*, *42*, 10.1002/2015GL064531.

Kim, E.-H., J. R. Johnson, H. Kim and D.-H. Lee (2015b), Inferring Magnetospheric Heavy Ion Density using EMIC waves, *J. Geophysics. Res.*, *120*, doi:10.1002/2015JA021092.

Kim, E.-H., S. A. Boardsen, J. R. Johnson and J. A. Slavin (2015c) ULF waves at Mercury, *in Low-frequency Waves in Space Plasmas*. American Geophysical Union, Washington, D. C.

Lee, D.-H., J. R. Johnson, K. Kim and K.-S. Kim (2008), Effects of heavy ions on ULF wave resonances near the equatorial region, *J. Geophys. Res.*, *113*, A11212, doi:10.1029/2008JA013088.

Lee, J. H. and Vassilis Angelopoulos (2015), Observations andmodeling of EMICwave properties in the presence of multiple ion species as function of magnetic local time, *J. Geophys. Res.*, *119*, 8942, doi:10.1002/2014JA020469.

Loto'aniu, T. M., R. M. Thorne, B. J. Fraser and D. Summers (2006), Estimating relativistic electron pitch angle scattering rates using properties of the electromagnetic ion cyclotron wave spectrum, *J. Geophys. Res.*, *111* , A04220, doi:10.1029/2005JA011452.

Min, K., J. Lee, K. Keika and W. Li (2012), Global distribution of EMIC waves derived from THEMIS observations, *J. Geophys. Res.*, *117*, A05219, doi:10.1029/2012JA017515.

Min, K., K. Liu, J. W. Bonnell, A. W. Breneman, R. E. Denton, H. O. Funsten, J.-M. Jahn, C. A. Kletzing, W. S. Kurth, B. A. Larsen, G. D. Reeves, H. E. Spence and J. R. Wygnant (2015), Study of EMIC Wave Excitation Using Direct Ion Measurements, *J. Geophys. Res.*, *120*, 2702–2719, doi: 10.1002/2014JA020717.

Miyoshi, Y., K. Sakaguchi, K. Shiokawa, D. Evans, J. Albert, M. Connors and V. Jordanova (2008), Precipitation of radiation belt electrons by EMIC waves, observed from ground and space, *Geophys. Res. Lett.*, *35*, L23101, doi:10.1029/2008GL035727.

Omidi, N., J. Bortnik, R. Thorne and L. Chen (2013), Impact of cold O+ ions on the generation and evolution of EMIC waves, *J. Geophys. Res.*, *118*, 434, doi:10.1029/2012JA018319.

Perraut, S., R. Gendrin, A. Roux and C. de Villedary (1984), Ion cyclotron waves - Direct comparison between ground-based measurements and observations in the source region, *J. Geophys. Res.*, *89*, 195-202.

Píša, D., M. Parrot, O. Santolík and J. D. Menietti (2015), EMIC waves observed by the low-altitude satellite DEMETER during the November 2004 magnetic storm, *J. Geophys. Res.*, *120*, doi:10.1002/2014JA020233.

Rauch, J. L. and A. Roux (1982), Ray tracing of ULF waves in a multicomponent magnetospheric plasma - Consequences for the generation mechanism of ion cyclotron waves, *J. Geophys. Res.*, *87*, 8191-8198.

Rönnmark, K. and M. André (1991), Convection of ion cyclotron waves to ion-heating regions, *J. Geophys. Res.*, *96*, 17573.

Saikin, A. A., J.-C. Zhang, R. C. Allen, C. W. Smith, L. M. Kistler, H. E. Spence, R. B. Torbert, C. A. Kletzing and V. K. Jordanova (2015), The occurrence and wave properties of H+-, He+-, and O+-band EMIC waves observed by the Van Allen Probes, *J. Geophys. Res.*, *120*, doi:10.1002/2015JA021358.

Sheeley, B. W., M. B. Moldwin, H. K. Rassoul and R. R. Anderson (2001), An empirical plasmasphere and trough density model: CRRES observations, *J. Geophys. Res.*, *106*, 25631.

Shprits, Y. Y., W. Li and R. M. Thorne (2006), Controlling effect of the pitch angle scattering rates near the edge of the loss cone on electron lifetimes, *J. Geophys. Res.*, *111*, A12206, doi:10.1029/2006JA011758.

Silin, I., I. R. Mann, R. D. Sydora, D. Summers and R. L. Mac (2011), Warm plasma effects on electromagnetic ion cyclotron wave MeV electron interactions in the magnetosphere, *J. Geophys. Res.*, *116*, A05215, doi:10.1029/2010JA016398.

Smith, R. L. and N. Brice (1964), Propagation in Multicomponent Plasmas, *J. Geophys. Res.*, *69*, 5029-5040.

Thorne, R. M. (2010), Radiation belt dynamics: The importance of wave-particle interactions, *Geophy. Res. Lett.*, *37*, L22107, doi:10.1029/2010GL044990.

Young, D. T., S. Perraut, A. Roux, C. de Villedary, R. Gendrin, A. Korth, G. Kremser and D. Jones (1981), Wave-particle interactions near Omega/He plus/ observed on GEOS 1 and 2. I - Propagation of ion cyclotron waves in He/plus/-rich plasma, *J. Geophys. Res.*, *86*, 6755-6772.

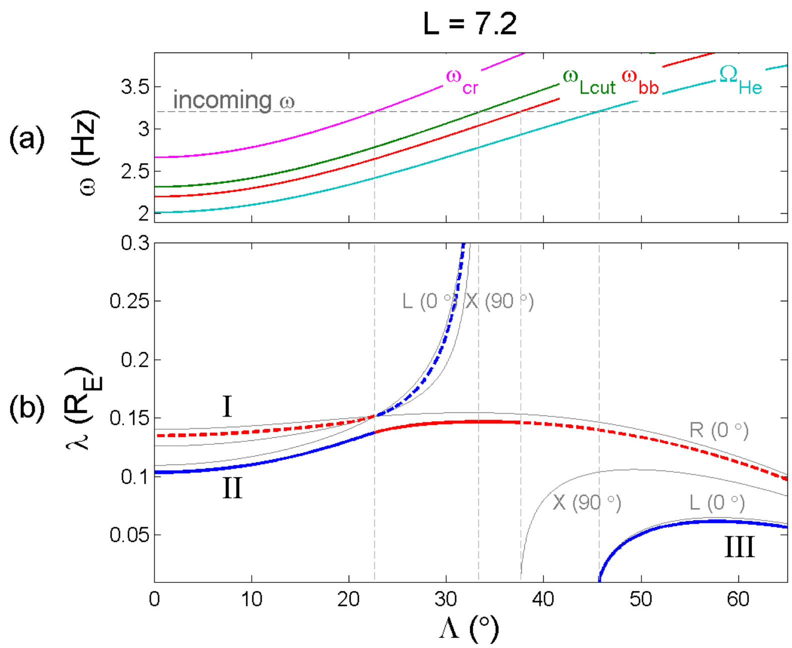

Figure 1. (a) The crossover (ω_{bb}, magenta), LHP wave cutoff (ω_{Lcut}, green), Buchsbaum resonance (ω_{bb}, red), and He^+ (Ω_{He}, cyan) gyrofrequencies based on a dipole magnetic field line with L = 7.2 assuming a 5% He^+ plasma using the electron density [*Denton et al.*, 2006]. The gray dashed line indicates the selected wave frequency for calculation of the dispersion relation; (b) Dispersion relation for ω=3.2Hz as a function of magnetic latitude (Λ) calculated by adopting the plasma conditions shown in Figure 1a. In this figure, parallel and perpendicular propagation are shown with gray solid lines. The colored line shows the dispersion relation with a wavenormal angle, θ_k = 25°. The two branches are labeled according to their polarization and propagation characteristics with right-hand (red), left-hand polarization (blue), guided (solid) and unguided (dashed lines), respectively. Here, the four gray dashed vertical lines are where wave frequency (ω) matches ω_{cr}, ω_{Lcut}, ω_{bb}, and Ω_{He}, respectively.

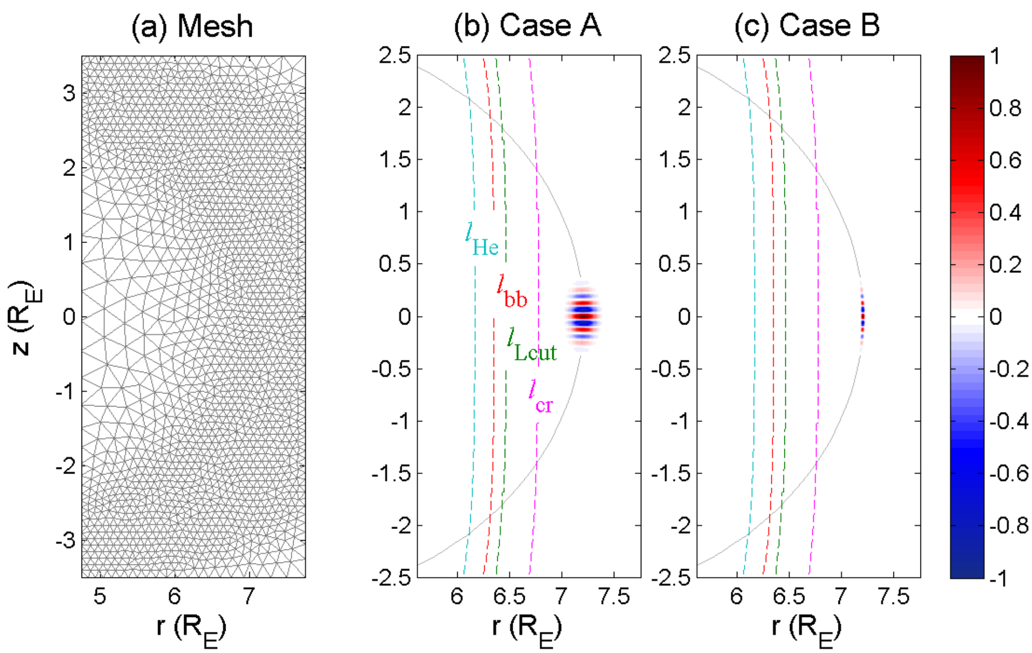

Figure 2. (a) Example of unstructured the density of the triangular mesh in the magnetosphere for $4.75 \leq L \leq 7.75$. In this figure, node and element numbers are 1747 and 3342, which are approximately 45 times fewer than the actual node and triangle numbers of 91384 and 181729 used for the calculation, although the relative density of elements is the same. (b)-(c) Contour plots of launched wave power. In order to examine how the wave normal angle near the magnetic equator affects to EMIC wave propagation, we perform two simulations with wide (Case A in Figure 2b) and narrow (Case B in Figure 2b) source width in the $\boldsymbol{\eta}$ direction as shown in Figure 2b and 2c, respectively. The lines marked with l_{He} (cyan dashed line), l_{bb} (red dashed line), l_{Lcut} (green dashed line), and l_{cr} (magenta dashed line) show locations where the wave frequency matches to the helium gyro- (Ω_{He}), Buchsbaum resonance (ω_{bb}), LHP wave cutoff (ω_{Lcut}), and crossover frequencies (ω_{cr}), respectively.

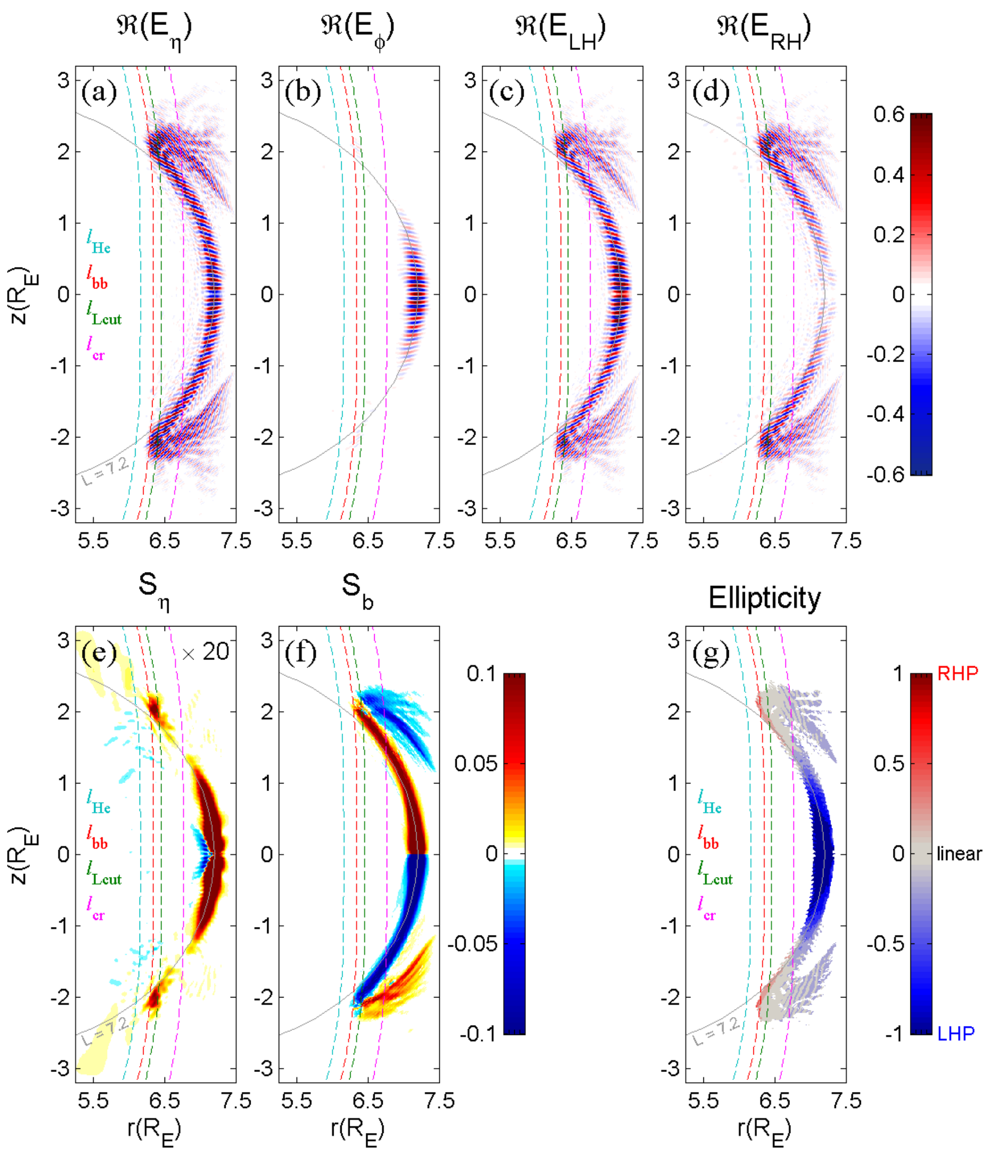

Figure 3. Wave solutions using the FW2D code for quasi-parallel propagating waves; (a) E_η, electric field normal direction to local magnetic field line, (b) E_φ, electric field azimuthal component, (c) E_{LH}, LHP component calculated using equation (4), (d) E_{RH}, RHP component calculated using equation (4), (e) S_η, Poynting flux normal direction to local magnetic field line, (f) S_b, field-aligned Poynting flux, and (g) ellipticity. Waves are initially launched near the magnetic equator at L=7.2 as LHP waves. The waves are well guided by $\mathbf{B}_0$, propagate to higher magnetic latitude, and reflect at the Buchsbaum resonance location.

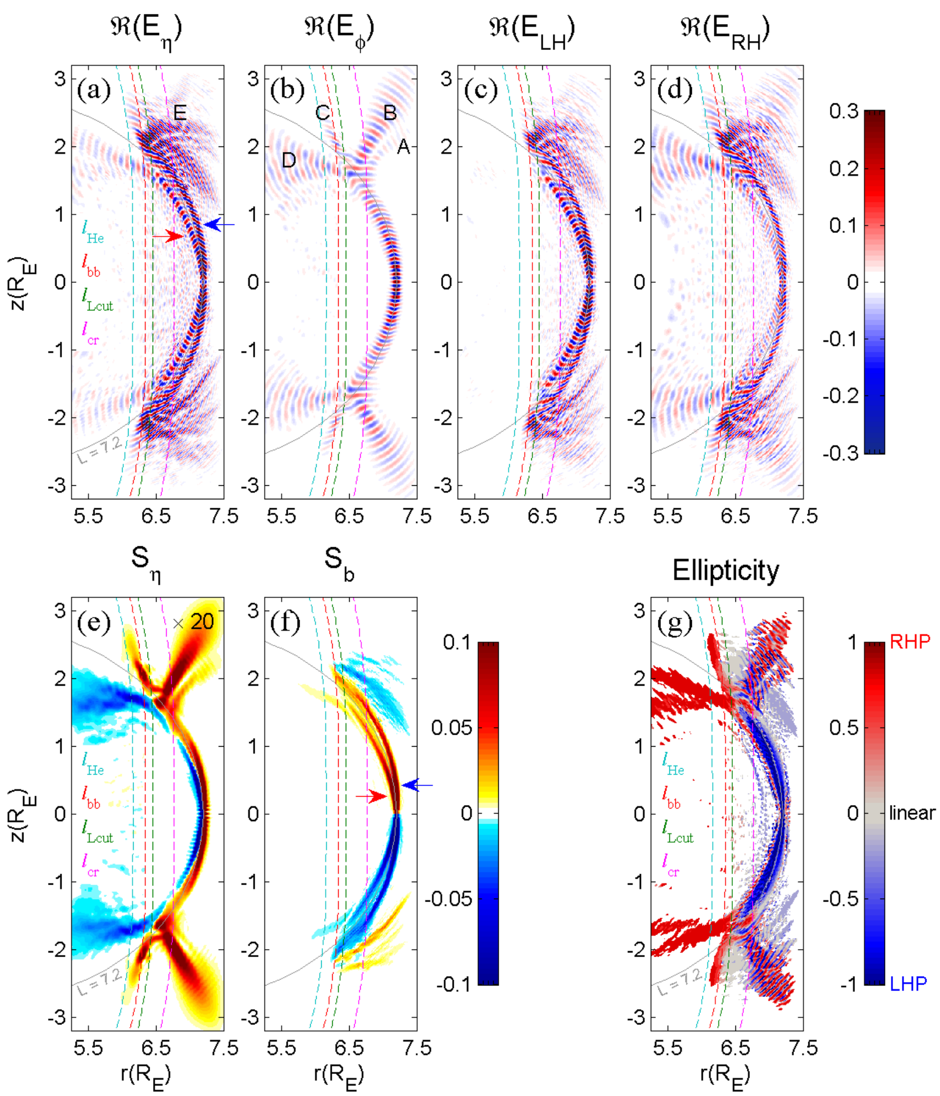

Figure 4. Wave solutions code for waves propagating with larger normal angle. In this figure, two rays propagate along the magnetic field line toward smaller (red arrow) and larger L-shell (blue arrow). For waves propagating toward smaller L-shell, mode conversion from earthward propagating LHP EMIC waves to magnetosonic waves at the crossover location occurs. The RHP magnetosonic waves (marked A in Figure 4b) propagate to the weaker magnetic field region (outer magnetosphere), while LHP magnetosonic waves propagate to the stronger magnetic field region from l_{cr} to l_{Lcut} where they reflect and propagate to the outer

magnetosphere (marked "B" in Figure 4b). At l_{cr}, polarization reversal from LHP to RHP also occurs. When RHP EMIC wave modes reach l_{bb}, these waves become unguided as shown in Figure 4 and disperse into the inner/outer magnetosphere (marked "C" and "D" in Figure 4b).

Movie S1. Time dependent wave solution of $E(r,z,t) = E(r,z)\exp(-i\omega t)$ for Case A; (a) E_η and (b) E_φ.

Movie S2. Time dependent wave solution of $E(r,z,t) = E(r,z)\exp(-i\omega t)$ for Case B; (a) E_η and (b) E_φ.

Princeton Plasma Physics Laboratory
Office of Reports and Publications

Managed by
Princeton University

under contract with the
U.S. Department of Energy
(DE-AC02-09CH11466)

P.O. Box 451, Princeton, NJ 08543
Phone: 609-243-2245
Fax: 609-243-2751

E-mail: publications@pppl.gov

Website: http://www.pppl.gov